

ILT3 (LILRB4) Promotes the Immunosuppressive Function of Tumor-Educated Human Monocytic Myeloid-Derived Suppressor Cells

Latika Singh¹, Eric S. Muise², Anannya Bhattacharya³, Jeff Grein⁴, Sarah Javaid², Peter Stivers¹, Jun Zhang³, Yujie Qu³, Barbara Joyce-Shaikh⁵, Andrey Loboda², Chunsheng Zhang², Michael Meehl⁶, Derek Y. Chiang², Sheila H. Ranganath¹, Michael Rosenzweig¹, and Philip E. Brandish¹



ABSTRACT

Myeloid-derived suppressor cells (MDSC) are immature myeloid cells that accumulate in the tumor microenvironment (TME). MDSCs have been shown to dampen antitumor immune responses and promote tumor growth; however, the mechanisms of MDSC induction and their role in promoting immune suppression in cancer remain poorly understood. Here, we characterized the phenotype and function of monocytic MDSCs (M-MDSC) generated by coculture of human peripheral blood mononuclear cells with SK-MEL-5 cancer cells *in vitro*. We selected the SK-MEL-5 human melanoma cell line to generate M-MDSCs because these cells form subcutaneous tumors rich in myeloid cells in humanized mice. M-MDSCs generated via SK-MEL-5 coculture expressed low levels of human leukocyte antigen (HLA)-DR, high levels of CD33 and CD11b, and suppressed both CD8⁺ T-cell proliferation and IFN γ secretion. M-MDSCs also expressed higher levels of immu-

noglobulin-like transcript 3 (ILT3, also known as LILRB4) and immunoglobulin-like transcript 4 (ILT4, also known as LILRB2) on the cell surface compared with monocytes. Therefore, we investigated how ILT3 targeting could modulate M-MDSC cell function. Treatment with an anti-ILT3 antibody impaired the acquisition of the M-MDSC suppressor phenotype and reduced the capacity of M-MDSCs to cause T-cell suppression. Finally, in combination with anti-programmed cell death protein 1 (PD1), ILT3 blockade enhanced T-cell activation as assessed by IFN γ secretion.

Implications: These results suggest that ILT3 expressed on M-MDSCs has a role in inducing immunosuppression in cancer and that antagonism of ILT3 may be useful to reverse the immunosuppressive function of M-MDSCs and enhance the efficacy of immune checkpoint inhibitors.

Introduction

T-cell checkpoint immunotherapies demonstrate significant clinical benefits and durable responses only in a subset of patients with certain tumors, such as melanoma and lung cancer (1, 2). However, most patients fail to respond to T-cell checkpoint immunotherapies. Several clinical studies have shown that high infiltration of suppressive myeloid cells in solid tumors correlates with poor response to checkpoint blockade therapies in most cancers (3–6). Using high-dimensional profiling technologies and single-cell RNA sequencing,

tumor-infiltrating myeloid populations have been identified in multiple cancer indications, such as clear cell renal cell carcinoma (ccRCC) and lung tumors, which are linked to immunosuppression, and in ccRCC to shorter progression-free survival (7, 8). Targeting the suppressive myeloid compartment is emerging as a compelling approach to overcome limitations of T-cell checkpoint inhibitors.

MDSCs comprise immature myeloid cells that are diverse in nature. They originate from myeloid progenitor cells and have been reported to expand and reside in the blood, lymphoid organs, and tumor tissues in several diseases, such as cancer, autoimmune diseases, and chronic inflammatory conditions (9–12). MDSCs can impact both innate and adaptive immune responses and cause immunosuppression. Clinical observations from patients with cancer showed a positive correlation between number of MDSCs in peripheral blood/tumor masses with tumor burden and clinical stage in several cancers (13, 14). In melanoma, circulating MDSCs are associated with the failure of T-cell checkpoint inhibitor therapy (6). Previously treated patients with metastatic urothelial carcinoma with comparable levels of tumor IFN γ experienced differential survival benefit with nivolumab depending on the MDSC levels detected in the treatment-naïve state. Interestingly, patients with high baseline circulating monocytic MDSC (M-MDSC) levels had a lower overall survival rate after treatment with nivolumab compared with those with lower circulating MDSC levels (15). A better understanding of the immunosuppressive functions of MDSCs can identify novel therapeutic targets for combination treatments that may improve clinical outcomes.

Tumor development may be associated with the accumulation of MDSCs in the tumor microenvironment (TME; ref. 16). These cells also promote tumor cell invasion, angiogenesis, and tumor growth (17). MDSCs reside in the peripheral blood mononuclear cell (PBMC) fraction in humans. Polymorphonuclear (PMN)-MDSCs are

¹Discovery Oncology, Merck & Co., Inc., Boston, Massachusetts. ²Genetics and Pharmacogenomics, Merck & Co., Inc., Boston, Massachusetts. ³Immunology, Merck & Co., Inc., Boston, Massachusetts. ⁴Genetics and Pharmacogenomics, Merck & Co., Inc., South San Francisco, California. ⁵Discovery Oncology, Merck & Co., Inc., South San Francisco, California. ⁶Biologics Discovery, Merck & Co., Inc., Boston, Massachusetts.

Note: Supplementary data for this article are available at Molecular Cancer Research Online (<http://mcr.aacrjournals.org/>).

E.S. Muise and A. Bhattacharya contributed equally to this article.

Current address for Barbara Joyce-Shaikh: Johnson & Johnson, San Diego, California; Current address for, M. Meehl, Jounce Therapeutics, Inc., Cambridge, Massachusetts; current address for Derek Y. Chiang, Bayer, Cambridge, Massachusetts; current address for Philip E. Brandish, Bicycle Therapeutics, Inc., Lexington, Massachusetts.

Corresponding Author: Latika Singh, Merck & Co., Inc., 33 Avenue Louis Pasteur, Boston, MA 02115. Phone:617-992-3145; E-mail: latika.singh@merck.com

Mol Cancer Res 2021;19:702-16

doi: 10.1158/1541-7786.MCR-20-0622

©2020 American Association for Cancer Research.

CD14⁻CD11b⁺CD15⁺ or CD14⁻CD11b⁺CD66b⁺ and M-MDSCs are CD14⁺ CD33⁺CD11b⁺ human leukocyte antigen (HLA)-DR^{-low} (18). Most importantly, MDSCs are functionally defined by their ability to inhibit T-cell activation and proliferation (12). MDSCs inhibit T-cell effector functions through a range of mechanisms that include expression of arginase (Arg-1), inducible nitric oxide synthase (iNOS), TGFβ, IL10, deprivation of L-cysteine, activation, and proliferation of regulatory T cells (Treg), synthesis of suppressive factors, including nitric oxide (NO), and generation of reactive oxygen species (ROS; refs. 12, 19). Numerous tumor-secreted factors have been implicated to induce MDSCs, including GM-CSF, IL6, PGE2, VEGF, IL10, and IL1β (12, 20, 21). A few studies have shown that MDSCs might be induced by coculturing human PBMCs or CD14⁺ monocytes *in vitro* with different cancer cell lines (22, 23); however, the mechanism of MDSC accumulation/expansion is poorly understood. In our study, we report for the first time that M-MDSCs induced by SK-MEL-5 cancer cells expressed high levels of inhibitory receptors ILT3 and ILT4 and low levels of HLA-DR, produced IL10, and suppressed T-cell activation and proliferation. We selected the SK-MEL-5 tumor cell line to generate M-MDSCs based on the data from *in vivo* mouse models (24; A.M. Torres-Adorno; submitted for publication).

Some studies suggest that MDSCs induce an anti-inflammatory, immunosuppressive, and protumorigenic environment by expressing immunoinhibitory receptors such as ILT3 and ILT4 (25, 26). Previous studies have shown that during pregnancy, HLA-G promotes MDSC accumulation in the placenta and suppressive activity via the ILT4 receptor (27). ILT3 is a related cell surface molecule of the immunoglobulin superfamily, which is expressed on monocytic myeloid cells such as monocytes, dendritic cells, macrophages, and MDSCs (28, 29). ILT3 functions as an inhibitory receptor, and its intracellular domain contains putative immunoreceptor tyrosine-based inhibitory (ITIM) motifs (30, 31). It is hypothesized that ILT3 keeps myeloid cells in an immature and suppressive state (32); however, the role of ILT3 in the acquisition and maintenance of immature and suppressive phenotype of M-MDSCs has not been studied. Our previous internal data from MSD with a human IgG4 chimeric variant of anti-ILT3, clone 52B8 (c52B8), in an SK-MEL-5-educated M-MDSC model led us to investigate ILT3 blockade in detail (33). We evaluated ILT3-specific monoclonal antibodies (mAbs) and found that ILT3 antagonism altered the suppressive function of M-MDSCs induced by soluble factors produced by SK-MEL-5 cells. SK-MEL-5-educated M-MDSCs treated with anti-ILT3 antibody have decreased levels of IL10 and CD163 and increased levels of programmed cell death protein 1 (PD-1) compared with the isotype control-treated cells. In addition, anti-ILT3 treatment enhanced TNFα secretion and increased the expression of an activation marker, CD86, in SK-MEL-5-educated M-MDSCs. ILT3 antagonism also relieved the suppressive effect of SK-MEL-5-educated M-MDSCs on T-cell proliferation and combines with PD1 blockade to enhance immune cell function.

Materials and Methods

SK-MEL-5 cell culture

The tumor cell line SK-MEL-5 was obtained from ATCC. The cells were grown in RPMI1640 supplemented with 10% heat-inactivated FBS (Hyclone, Inc.), 2 mmol/L L-glutamine, 50 U/mL each of penicillin/streptomycin, in a humidified incubator maintained at 37°C with 5% CO₂. After thawing, cells were used for up to 8–10 passages and their authenticity was checked by short tandem repeat analysis at IDEXX Laboratories, Inc. The cells were routinely checked for *Mycoplasma* contamination using a polymerase chain reaction method that

included primers that hybridize with a conserved region of the *Mycoplasma* genome. The most recently confirmed negative test result for *Mycoplasma* contamination was on September 3, 2020, at Analytical Biological Services Inc.

Measurement of tumor-derived factors by ELISA

For quantifying cytokines and growth factors secreted by SK-MEL-5 cells, 1 million cells were seeded in a 6-well tissue culture plate with 2 mL RPMI supplemented with glutamine and 10% heat-inactivated FBS. After 3 days, conditioned media were collected and passed through a 0.2-μm syringe filter unit to remove cell debris and stored in aliquots at -20°C prior to the analysis. For assessing the concentrations of IL1β, IL6, IL8, IL10, IL13, and TNFα, the V-PLEX Proinflammatory Panel 1 Human Kit (Meso Scale Discovery) was used according to the manufacturer's instructions. For quantifying GM-CSF and VEGF concentrations, a customized kit (Meso Scale Discovery) was used. All kits were developed on the basis of a multiplexed electrochemiluminescence system, and light intensity was measured by SECTOR Imager S 6000.

Peripheral blood mononuclear cell isolation

Peripheral blood mononuclear cells (PBMC) were isolated from healthy human peripheral blood leukopaks using Lymphopreps (STEMCELL Technologies) via density-gradient centrifugation according to the manufacturer's instructions.

Generation of human myeloid-derived suppressor cells and macrophages

To generate cancer cell line-educated M-MDSCs, healthy human PBMCs from individual donors were cultured in cell culture medium (20 × 10⁶ cells in 25 mL RPMI1640 supplemented with 10% heat-inactivated FBS, 2 mmol/L L-glutamine, 50 U/mL each of penicillin/streptomycin) with SK-MEL-5 tumor cells (4 × 10⁵ cells in a final volume of 25 mL) in the presence of 20 ng/mL GM-CSF (R&D Systems) at 37°C for 7 days. For cytokine-induced MDSCs, healthy human PBMCs were cultured (20 × 10⁶ cells in 25 mL volume) in media containing GM-CSF (20 ng/mL; R&D Systems) and IL6 (20 ng/mL; R&D Systems) for 7 days. PBMCs cultured in medium alone served as a negative control for each donor. Media supplemented with fresh cytokines was replaced on day 4. After coculturing for 7 days, cells were harvested using Detachin solution (Genlantis), and CD33⁺ myeloid cells were isolated using anti-CD33 magnetic microbeads and LS column separation (Miltenyi Biotec) according to the manufacturer's instructions. More than 90% of isolated cell populations tested positive for CD33 expression by flow cytometry analysis. The viability of isolated cells was confirmed using Trypan blue dye exclusion assay. M2 Macrophages were differentiated using ImmunoCult-SF Macrophage media (STEMCELL Technologies) supplemented with M-CSF (50 ng/mL; STEMCELL Technologies) for 5 days. On day 5, macrophages were polarized by adding IL4 (10 ng/mL; STEMCELL Technologies) for 48 hours.

Phenotyping of human myeloid-derived suppressor cells

In vitro-generated M-MDSCs were characterized for expression of myeloid, antigen-presenting, and suppressor cell markers using flow cytometry. The cells (2 × 10⁵) from cocultures were detached from flasks using Detachin and stained with Fixable viability stain 510 (BD Biosciences) in DPBS in the dark on ice for 20 minutes and washed with 1 × wash buffer (10% BSA, 40 mmol/L EDTA, 1 × PBS). Next, the cells were incubated with human Fc receptor blocking solution FcX (diluted in staining buffer, 1:250, BD Biosciences) in the dark on ice for

10 minutes, and stained with a cocktail of fluorescently conjugated antibodies (0.2 µg each of CD14, CD11b, CD66b, 0.04 µg of CD33, 0.025 µg of HLA-DR, 0.1 µg each of anti-ILT3 clone ZM4.1, anti-ILT4 1E1, CD86, and CD45 in 100 µL staining buffer; Supplementary Table S1) for 30 minutes on ice in the dark. After the incubation, the cells were washed and resuspended in $1 \times$ DPBS. All samples were acquired on an LSR II flow cytometer using FACSDiva software (BD Biosciences). All flow cytometry data was analyzed using FlowJo software (FlowJo LLC) and GraphPad Prism 8. Binding signals were calculated as median fluorescence intensity (MFI) for each antibody.

Measurement of surface expression of ILT3 in SK-MEL-5 tumors in humanized (hu) NSG mice

All animal work was reviewed and approved by MSD IACUC before experiments were conducted. Female hu-NSG mice from 2 different human donors were purchased from The Jackson Laboratory. SK-MEL-5 cells (1×10^6 /mouse) were injected subcutaneously (SC) in hu-NSG mice at approximately 20 weeks of age. Study was randomized by tumor size and donor and tumors were measured in blinded fashion. SK-MEL-5 tumors in hu-NSG mice ($n = 5$) were collected 11 days after tumor cell implantation. Tumors were minced finely with a scalpel and digested using digestion medium containing 8 mL of RPMI1640 medium, 40 µL of 100 mg/mL collagenase I (Thermo Fisher Scientific Inc.), and 320 µL of 10,000 U/mL DNase I (Thermo Fisher Scientific Inc.) for 30 minutes at 37°C to obtain single-cell suspensions. Samples were filtered, red blood cells were removed by ACK lysis (Lonza), and cell numbers were counted using the ViCell Cell Viability Analyzer (Beckman Coulter).

One million (10^6) viable cells per tube were stained for viability using Fixable viability dye eFluor 506 (BD Biosciences) in DPBS followed by fluorescently labeled antibodies [0.25 µg of CD11b, 1 µg each of CD3, CD66b, CD33, 0.5 µg each of CD45, CD56, CD14, anti-ILT3 clone ZM4.1, or mouse IgG1 isotope control in FACS staining buffer on ice (Supplementary Table S2)]. The samples were analyzed as described previously for phenotyping of human M-MDSCs. Expression of ILT3 was calculated as the frequency of cells showing greater fluorescence signal when incubated with anti-ILT3 clone ZM4.1 than those incubated with the mouse IgG1 isotype control antibody.

Assessment of T-cell proliferation and IFN γ levels in myeloid-derived suppressor cell/T-cell coculture

Autologous CD8⁺ T cells were isolated from healthy human PBMCs using Easy Sep Human CD8⁺ T cell Enrichment Kit (negative selection) using the automated Robosep protocol (STEMCELL Technologies) according to the manufacturer's instructions. Purified CD8⁺ T cells (1×10^5 cells per well) were cultured alone or cocultured with CD33⁺ M-MDSCs isolated using anti-CD33 magnetic microbeads and LS column separation (Miltenyi Biotec) as described previously at the ratio of 8:1, 4:1, 2:1, and 1:1 (T cell:MDSC) or monocytes at the ratio of 4:1 (T cell:monocyte) in cell culture medium in 96-well U-bottom plates. T-cell proliferation was induced with anti-CD3/CD28 dynabeads (Thermo Fisher Scientific Inc.) or plate-bound anti-CD3 (OKT3, Thermo Fisher Scientific Inc.) and anti-CD28 (Fitzgerald) antibody and 100 U/mL IL2 (Thermo Fisher Scientific Inc.) and incubated at 37°C for 3 days. IFN γ levels in culture supernatants were determined using Mesoscale Discovery kits following the manufacturer's protocol. T-cell proliferation was analyzed using 3H-thymidine uptake assay. 0.5 pCi/well 3H-thymidine (NEN Life Sciences) diluted in RPMI1640 was added to cells. After incubating the plates at 37°C for 4 hours, cells were harvested onto filter papers using an automated cell harvester (Perkin Elmer; ref. 34). Following this, scintillation fluid was

added, and counting was performed using a Beckman LS 6000IC scintillation counter. Results are expressed in counts/minute (CPM; ref. 34).

Real-time RT-PCR for gene expression of human myeloid-derived suppressor cells and monocytes

For real-time PCR analysis, SK-MEL-5-educated live CD45⁺ CD14⁺ CD33⁺ cells were isolated from tumor cell PBMC cocultures and human PBMCs from healthy individual donors by FACS, and mRNA was isolated from cells using the PicoPure RNA isolation method, according to the manufacturer's protocol (Thermo Fisher Scientific Inc.). mRNA was treated with DNase and reverse-transcribed using QuantiTect Reverse Transcription according to the manufacturer's instructions (Qiagen). TaqMan assays were obtained commercially (Thermo Fisher Scientific) and gene specific preamplification was performed on 10 ng cDNA using TaqMan PreAmp according to the manufacturer's instructions (Thermo Fisher Scientific Inc). Real-time quantitative PCR was then performed on the Fluidigm Biomark using 20 \times TaqMan assays with TaqMan Fast Universal PCR Master Mix with no AmpErase UNG. Samples and primers were run on a 96.96 Dynamic Array according to the manufacturer's instructions (Fluidigm). Ubiquitin levels were measured in a separate reaction and were used for normalizing the data by the ΔC_t method. Normalized values were calculated with the following equation, using the mean cycle threshold value for ubiquitin and the gene of interest for each sample.

$$1.8^{-(Ct \text{ ubiquitin} - Ct \text{ gene of interest})} \times 10^4$$

Log₂ transformed expression values were used to perform a *t* test yielding fold change and corrected *P* values [false discovery rate, Benjamini-Hochberg; "*P*_{adj} (BH)"] using Omicsoft Array Studio (v10.0.1.118; monocytes, $n = 10$ samples; M-MDSC, $n = 12$ samples).

Generation of highly selective antibodies

Human IgG4 chimeric variant of anti-ILT3 clone 52B8 (c52B8) or a humanized IgG4 variant (h52B8) and isotype control human IgG4 were generated internally at MSD (33). Human IgG4 variant of anti-ILT4 clone 1E1 was generated in-house and described in U.S. Patent no. 2018/0298096 A1. Pembrolizumab is a humanized anti-PD1 antibody described in U.S. Patent no. 8354509 and WO2009/114335.

Transcriptome analysis of human myeloid-derived suppressor cells treated with anti-ILT3

Human PBMCs from healthy individual donors (2×10^6 cells per well) were cocultured with tumor cell line SK-MEL-5 (4×10^4 cells per well) in 6-well flat-bottom tissue culture plates in cell culture medium in the presence of 20 ng/mL GM-CSF (R&D Systems) at 37°C for 7 days. The cells were treated with isotype control hIgG4 or anti-ILT3 antibody c52B8 (1 µg/mL) for 7 days. SK-MEL-5-educated live CD45⁺ CD14⁺ CD33⁺ cells were isolated from tumor cell PBMC cocultures by FACS, and mRNA was isolated from cells using the PicoPure RNA Isolation method, according to the manufacturer's protocol (Thermo Fisher Scientific Inc.). For RNA sequencing, the Agilent TruSeq stranded total RNA kit (catalog no. RS-122-2201) was used for library preparation (Illumina). The resulting cDNA libraries were sequenced as previously described by Zhou and colleagues on an Illumina (HiSeqTM 4000) using a 50-base paired-end run (35). Cleaned reads were aligned to the Human.B38 genome reference using the Omicsoft Aligner (Qiagen) and using Ensembl.R86 gene models. Normalization of gene counts and differential expression analysis were performed using the R package DESeq2 (v1.22.2) yielding fold change and

corrected *P* values (false discovery rate, Benjamini–Hochberg; FDR_BH). A cutoff of 50 normalized counts in any replicate group was applied when identifying a gene signature to remove genes with very low expression. Heatmaps and box plots were created using Omicsoft Array Studio (Qiagen). GEO accession number GSE160401 (<https://www.ncbi.nlm.nih.gov/geo/query/acc.cgi?acc=GSE160401>).

Modulation of proinflammatory cytokine secretion by anti-ILT3 in human PBMC and SK-MEL-5 cocultures

Human PBMCs isolated from healthy individual donors (1×10^5 cells per well) were cocultured with tumor cell line SK-MEL-5 (2×10^3 cells per well) in 96-well flat-bottom tissue culture plates in cell culture medium in the presence of 20 ng/mL GM-CSF (R&D Systems) at 37°C for 5 days. The cells were treated with isotype control hIgG4 or anti-ILT3 antibody c52B8 (1 µg/mL) for 5 days. The supernatants were collected, and proinflammatory cytokine production was determined using MSD ELISA according to the manufacturer’s instructions (Meso Scale Discovery).

Activation of costimulatory molecule CD86 by anti-ILT3 in human PBMC and SK-MEL-5 cocultures

Human PBMCs and SK-MEL-5 cocultures were set-up as described in the section “transcriptome analysis of human myeloid-derived suppressor cells treated with anti-ILT3”. The cells were stained and analyzed for expression of CD86 as described previously for phenotyping of human M-MDSCs.

***In vitro* activity of anti-ILT3 and anti-PD1 and their combination in myeloid-derived suppressor cell and T-cell assay**

To assess the single-agent activity of anti-ILT3 on reversal of T-cell suppression induced by MDSCs, PBMC- SK-MEL-5 cocultures were repeated in the presence of 1 µg/mL hIgG4 or 1 µg/mL anti-ILT3 antibody. Autologous CD8⁺T cells (1×10^5 cells per well) were cultured alone or cocultured with purified CD33⁺ myeloid-suppressive cells at the ratio of 2:1, 4:1, and 8:1 (T cell:MDSC) in 96-well U-bottom plates for 30 minutes, in the presence of hIgG4 (1 µg/mL) or anti-ILT3 antibody c52B8 (1 µg/mL). After the preincubation, T-cell proliferation was induced with anti-CD3/CD28 beads (Thermo Fisher Scientific Inc.) and 100 U/mL IL2 (Thermo Fisher Scientific Inc.) and incubated at 37°C for 3 days. IFNγ levels in culture supernatants were determined using Mesoscale Discovery kits according to the manufacturer’s protocol. To assess the potential of anti-ILT3 antibody h52B8 or pembrolizumab, alone or in combination, to enhance T-cell function, autologous CD8⁺ T cells (1×10^5 cells per well) were cultured alone or cocultured with CD33⁺ myeloid-suppressive cells at the ratio of 8:1 (T cell:MDSC) in 96-well plates for 30 minutes, in the presence of either hIgG4 (1 µg/mL) or pembrolizumab (2 µg/mL) or h52B8 (1 µg/mL) or h52B8 (1 µg/mL) and pembrolizumab (2 µg/mL). After the preincubation, T-cell proliferation was induced as described above. Culture supernatants were harvested on day 2 for ELISA analysis of IFNγ secretion.

Statistical analysis

The half maximal effective concentration (EC₅₀) values were calculated using GraphPad Prism 7 (GraphPad software, Inc.). Nonlinear regression (4-parameter) fitting was used for graphing and calculation. Average and SD values were calculated using Microsoft Excel. Data were compared using *t* test or one-way ANOVA followed by Tukey multiple-comparisons test or one-way ANOVA followed by Dunnett correction when all data were compared with a control group. All analyses were conducted using

GraphPad Prism 8. Data were considered statistically significant at a *P* value less than 0.05.

Results

SK-MEL-5 cells express multiple MDSC-promoting factors

To identify and explore the role of soluble factors produced by tumor cells and their association with MDSC differentiation in the SK-MEL-5 and human PBMC coculture model (Fig. 1A), we assessed a panel of cytokines in the conditioned media using the Meso Scale Discovery immunoassay platform. We found increased levels of IL6, VEGF, IL8, and GM-CSF in the conditioned media from SK-MEL-5 cells compared with media control (Fig. 1B and C). IL13 and IL1β levels were low in the conditioned media. A previous study showed that treatment of human PBMCs with GM-CSF and IL6 induced CD33⁺ MDSCs with potent suppressive capacity *in vitro* (21). They were also able to generate CD33⁺ MDSCs when human PBMCs were cultured with GM-CSF and IL1β or VEGF (21).

SK-MEL-5 tumor cells promote the differentiation of M-MDSC population from human PBMCs *in vitro*

To explore the impact of SK-MEL-5 tumor cells on MDSC differentiation, we cocultured human PBMCs isolated from healthy donors with SK-MEL-5 cancer cells in the presence of GM-CSF (Fig. 1A). The resulting myeloid cell fraction was characterized with respect to cell surface phenotype, T-cell suppression, and gene expression profile. After 7 days of coculture, SK-MEL-5-educated myeloid cells demonstrated a monocytic MDSC-like phenotype, characterized by similar cell surface expression of CD14, increased levels of CD33 and CD11b, and decreased expression of HLA-DR compared with PBMCs cultured in medium alone for 7 days. (Fig. 1D and E; Supplementary Fig. S1A–S1C). The absence of CD66b, a bona fide granulocytic marker, confirmed that SK-MEL-5-educated cells were M-MDSCs (Supplementary Fig. S1C). To compare the phenotype of SK-MEL-5-educated M-MDSCs with cytokine-induced M-MDSCs, we differentiated human PBMCs in the presence of cytokines GM-CSF and IL6. We found SK-MEL-5-educated M-MDSCs exhibited a similar phenotype to the cytokine-induced M-MDSCs with low-level expression of HLA-DR; however, cytokine-induced M-MDSCs expressed lower levels of CD14 (Supplementary Fig. S1D). These results are consistent with previous findings that GM-CSF and IL6 reduce CD14 expression on M-MDSCs (21). SK-MEL-5-educated M-MDSCs exhibited significantly lower expression of HLA-DR compared with M2 macrophages, suggesting that SK-MEL-5-educated monocytes do not differentiate into macrophages (Supplementary Fig. S1E). These results corroborate previous findings that the monocytes differentiated using conditioned media from the renal cell carcinoma cell line 786.O had lower expression of HLA-DR compared with M2 macrophages (12). In addition, we looked at the expression of two inhibitory receptors, ILT3 and ILT4, because previous studies reported the expression of these two markers on MDSCs (27, 29, 36). Moreover, it is hypothesized that ILT3 plays a role in maintaining immature and suppressive phenotype in MDSCs, although the latter has not been experimentally proven. We found that ILT3 and ILT4 expression was elevated on SK-MEL-5-educated M-MDSCs compared with monocytes (Fig. 1F and G). In addition, SK-MEL-5-educated M-MDSCs had higher expression of ILT3 compared with CD14⁺ monocytes from PBMCs cultured in medium alone for 7 days (Supplementary Fig. S1C). Our data, therefore, suggests that SK-MEL-5-educated monocytes phenotypically resemble M-MDSCs. We have developed and previously reported an *in vivo* model using human SK-MEL-5 tumor cells grown

Downloaded from <http://aacrjournals.org/ncr/article-pdf/19/4/702/3101820/702.pdf> by guest on 10 February 2024

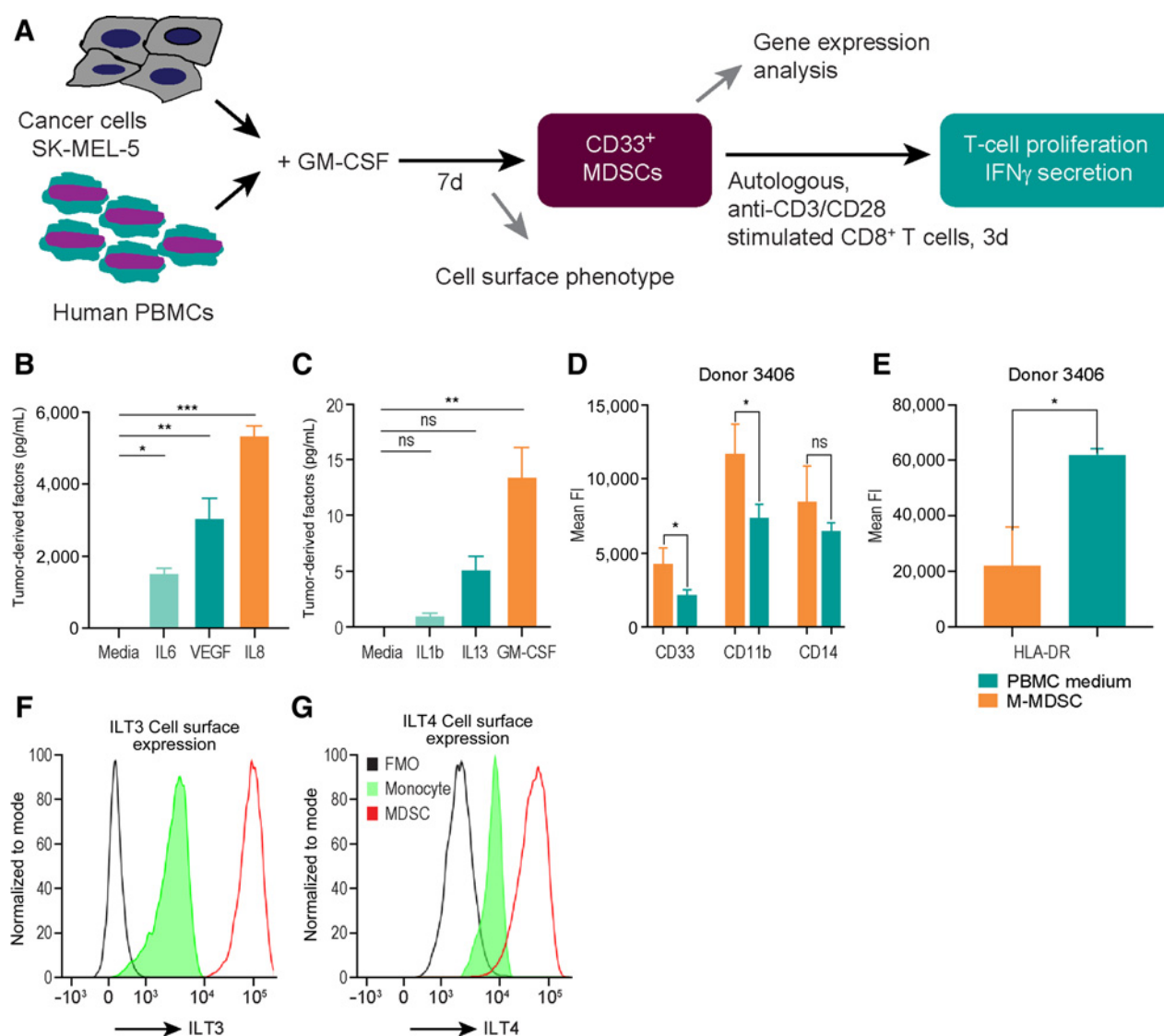


Figure 1.

SK-MEL-5-derived soluble factors promote monocyte to M-MDSC differentiation. **A**, Schematic illustration of the SK-MEL-5-PBMC coculture system and *in vitro* differentiation of monocytes into monocytic MDSCs. **B** and **C**, Soluble factors in SK-MEL-5 tumor cell line supernatants. The results are expressed as average \pm SD from two independent studies with two technical replicates each and one-way ANOVA followed by Dunnett correction was used to calculate *P* value (*, *P* < 0.05; **, *P* < 0.005; ***, *P* < 0.0005; n.s., not statistically significant). **D** and **E**, Mean fluorescence intensity (MFI) of cell surface expression of CD33, CD11b, CD14 and HLA-DR on SK-MEL-5-educated M-MDSCs and normal myeloid counterparts from PBMCs cultured in medium alone. Representative data of one out of two PBMC donors are shown. At least 2 independent experiments were performed with two PBMC donors. Bar plots are represented as average \pm SD and *t* test was used to calculate *P* value (*, *P* < 0.05; n.s., not statistically significant). **F** and **G**, ILT3 and ILT4 expression on CD45⁺/CD33⁺/CD14⁺ MDSCs and monocytes using flow cytometry. Cells that were stained with all fluorochromes except anti-ILT3 or anti-ILT4 were used as a negative control (Fluorescence minus one "FMO"). The results are expressed as MFI from 2 PBMC donors.

in mice with a humanized immune system (24). We observed that SK-MEL-5 tumors from all the different donor mice are rich in CD14⁺ myeloid cells that express ILT3 (Supplementary Fig. S2A and S2B) and ILT4 (A.M. Torres-Adorno; submitted for publication). Furthermore, we curated the Zilionis and colleagues' single-cell RNA-sequencing dataset from human lung tumors for the expression of the gene for ILT3, *LILRB4* and ILT4, *LILRB2* and found that *LILRB4* is predominantly expressed on monocytic myeloid cells, while *LILRB2* is expressed on both monocytic and granulocytic myeloid cells (Supplementary Fig. S3A–S3C; ref. 7). We analyzed the expression of *LILRB4* in The

Cancer Genome Atlas (TCGA) database using *in silico* deconvolution of bulk RNA-sequencing data (37) to establish the association between *LILRB4* expression and myeloid gene signature. We found that *LILRB4* is highly expressed on monocytic myeloid cells in several solid tumors including head and neck, kidney clear cell, lung adenocarcinoma, and pancreatic cancer (Supplementary Fig. S4). Previous studies have shown that M-MDSCs can suppress polyclonal (non-antigen-specific) T-cell responses (17, 38) and suppression of T-cell function is the definitive characteristic of MDSCs. We, therefore, assessed whether SK-MEL-5-educated M-MDSCs can suppress

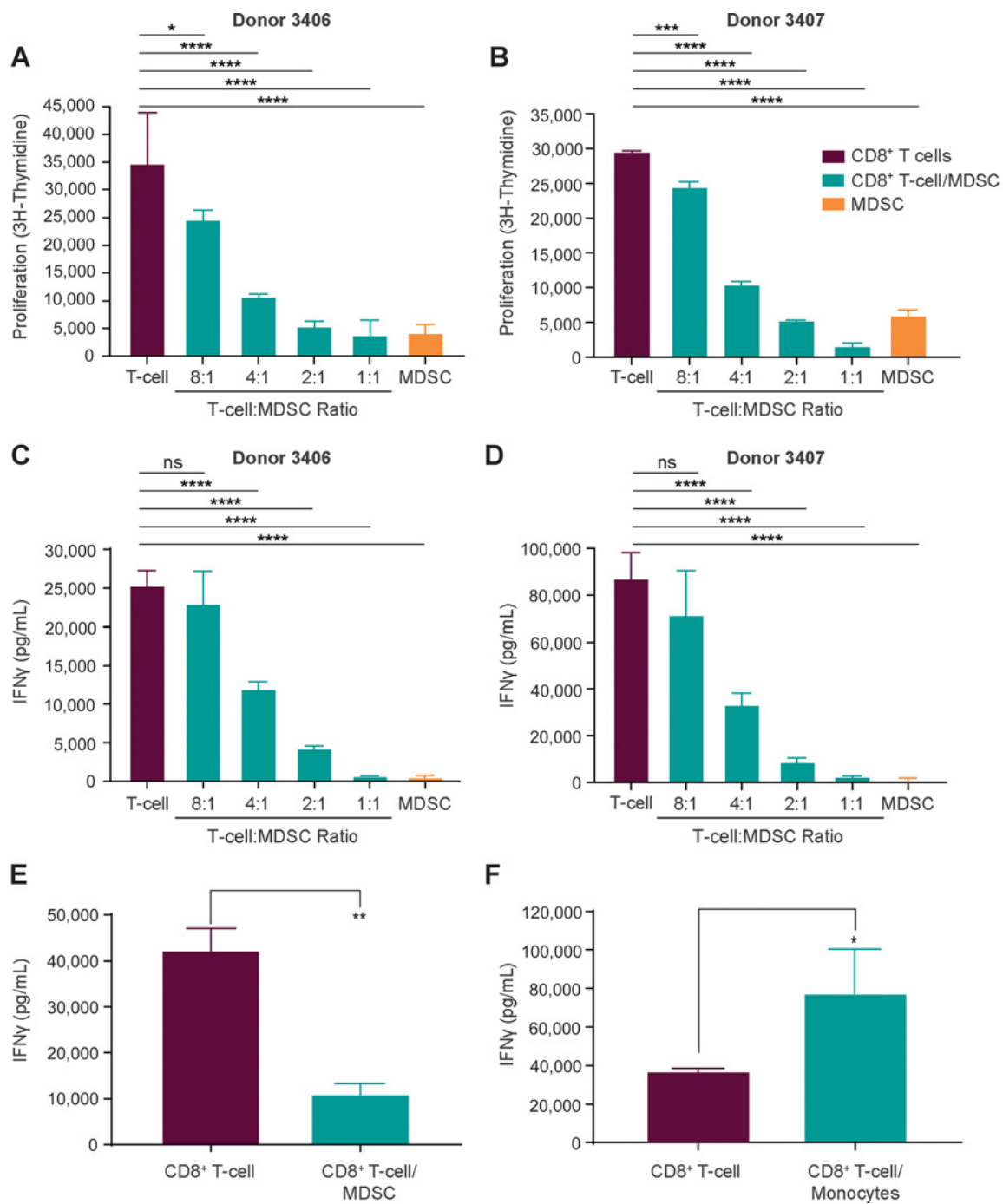
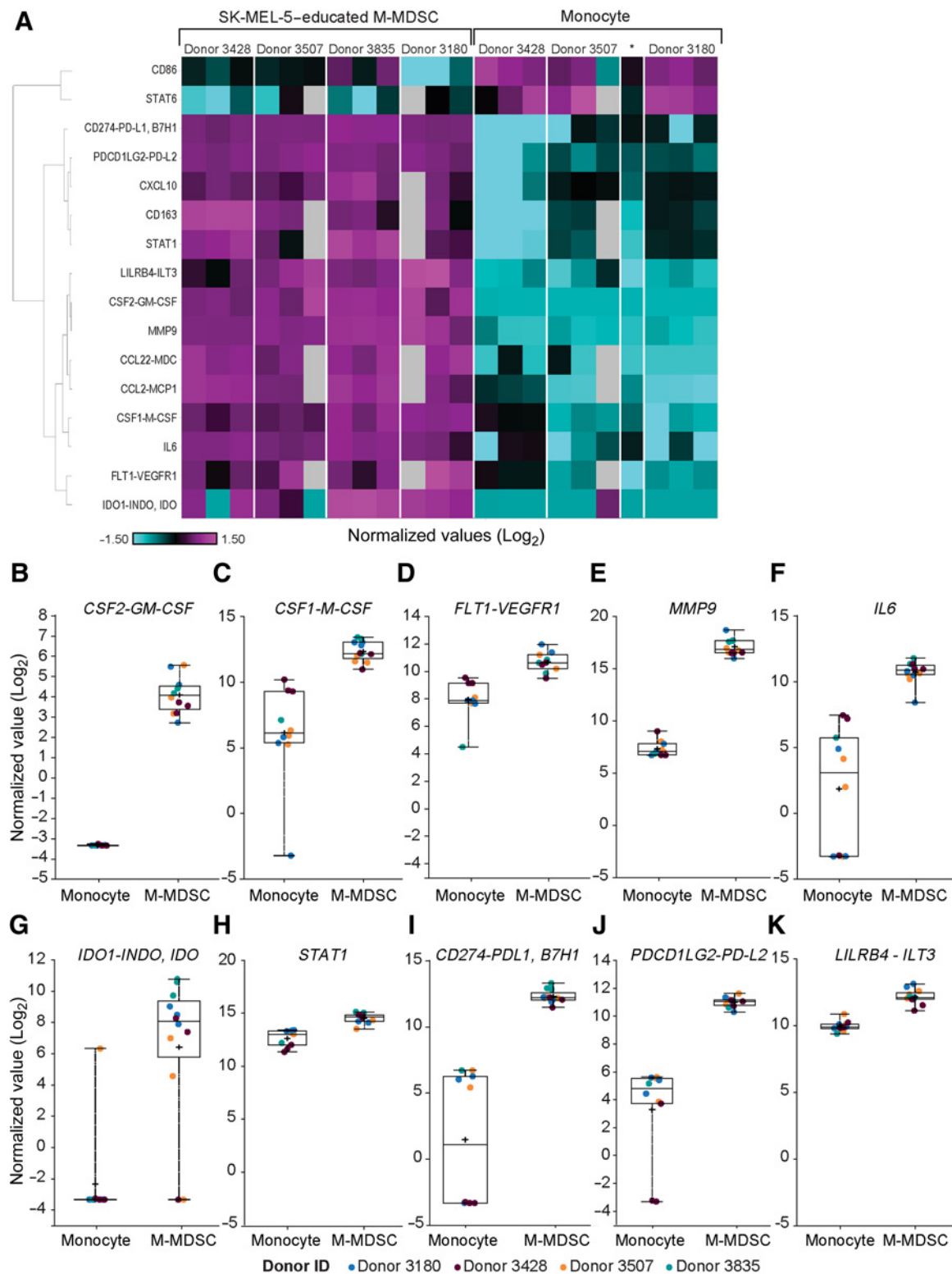


Figure 2. Suppression of autologous CD8 $^+$ T-cell proliferation by M-MDSCs (T cell:MDSC ratio: 8:1, 4:1, 2:1, 1:1). CD8 $^+$ T cells were stimulated with anti-CD3/CD28 beads and incubated with or without M-MDSCs for 3 days. **A** and **B**, T-cell proliferation was analyzed using 3H-thymidine uptake assay. The results are expressed as average \pm SD from two technical replicates ($n = 2$ PBMC donors), and one-way ANOVA followed by Dunnett correction was used to calculate P value (*, $P < 0.05$; ****, $P < 0.0005$; *****, $P < 0.0001$). **C** and **D**, The concentration of IFN γ was determined in supernatants collected from aforementioned CD8 $^+$ T-cell and M-MDSC cocultures. Data are shown from two independent experiments and are presented as average \pm SD from two technical replicates each ($n = 2$ PBMC donors), and one-way ANOVA followed by Dunnett correction was used to calculate P value (****, $P < 0.0001$; n.s., not statistically significant). **E**, CD8 $^+$ T cells were stimulated with plate-bound anti-CD3/CD28 antibody and incubated with or without M-MDSCs at 4T:1MDSC ratio for 3 days and IFN γ concentration was determined in supernatants. The results are expressed as average \pm SD from three technical replicates, and paired t test was used to calculate P value (**, $P < 0.005$). **F**, Activation of autologous CD8 $^+$ T-cell proliferation by monocytes (T cell:monocyte ratio 4:1). CD8 $^+$ T cells were stimulated with anti-CD3/CD28 beads and incubated with or without monocytes for 3 days and IFN γ concentration was determined in supernatants. The results are expressed as average \pm SD from two technical replicates in each experiment ($n = 3$ PBMC donors; *, $P < 0.05$; paired t test).

Downloaded from <http://aacrjournals.org/mcr/article-pdf/19/4/702/3101820/702.pdf> by guest on 10 February 2024

**Figure 3.**

Differentially expressed genes (DEG) between SK-MEL-5-educated M-MDSCs and monocytes. **A**, qRT-PCR analysis of selected genes in M-MDSCs and monocytes ($n = 4$ PBMC donors). The results are derived from three technical replicates at the level of the M-MDSC differentiation. The color gradient represents the normalized values (normalized to Ubiquitin B, center-scaled, Log₂). Gray, missing data. *, Donor 3835 one sample. **B-K**, Gene expression levels (normalized values, Log₂) of *CSF2-GM-CSF*, *CSF1-M-CSF*, *FLT1-VEGFR1*, *MMP9*, *IL-6*, *IDO1-INDO*, *IDO*, *STAT1*, *CD274-PDL1*, *B7H1*, *PDCD1LG2-PDL2*, *LILRB4-ILT3* in M-MDSCs and monocytes ($n = 4$ PBMC donors). All with $P < 0.0001$ (t test).

autologous T-cell proliferation (assessed by incorporation of tritiated thymidine) and IFN γ secretion in response to polyclonal stimulation. We cocultured autologous CD8⁺ T cells stimulated with anti-CD3/CD28 antibody-coupled beads and IL2 with M-MDSCs at a ratio of 8:1, 4:1, 2:1, and 1:1. SK-MEL-5-educated M-MDSCs suppressed both autologous T-cell proliferation and IFN γ secretion with increasing number of M-MDSCs (Fig. 2A–D). SK-MEL-5-educated M-MDSCs suppressed CD8⁺ T-cell proliferation by more than 80% at the 1:1 (T cell: M-MDSC) ratio, 70% at the 2:1 ratio, 60% at the 4:1 ratio, and 15% at the 8:1 ratio in both PBMC donors (Fig. 2A and B). Similar trends were observed with respect to IFN γ secretion (Fig. 2C and D). In comparison, GM-CSF/IL6 alone yielded a CD33⁺ cell population that was only mildly suppressive. We found that cytokine-induced M-MDSCs did not suppress CD8⁺ T-cell proliferation at the 8:1 (T cell: M-MDSC) ratio and caused milder CD8⁺T-cell suppression <50% at the 4:1 ratio in both the donors when compared with the SK-MEL-5-educated M-MDSCs. (Supplementary Fig. S5A and S5B). We found that CD33⁺ cells from PBMCs cultured in medium alone were not suppressive (Supplementary Fig. S6A and S6B).

In case M-MDSCs were phagocytosing the anti-CD3/CD28 antibody-coated beads before T-cell activation, which would lead to a false positive result, we stimulated the T cells with plate bound anti-CD3/CD28 antibody and IL2 instead of anti-CD3/CD28 antibody-coupled beads and IL2 during coculture with the M-MDSCs. SK-MEL-5-educated M-MDSCs demonstrated similar potent T-cell suppression (70%) in the presence of plate bound anti-CD3/CD28 antibody at 4 T cell:1 M-MDSC ratio (Fig. 2E). In contrast, robust T-cell activation and IFN γ secretion were observed when monocytes were cocultured with anti-CD3/CD28 stimulated T cells (Fig. 2F) and this highlights the fact that the suppressive function is acquired during coculture, not simply a general effect of adding monocytic cells to the T-cell assay.

Following phenotypic and functional characterization of SK-MEL-5-educated M-MDSCs, we profiled this cell population to identify molecular markers that distinguish M-MDSCs from monocytes on a transcriptional level using human immune and myeloid-based panels of 458 probes (representing 385 genes). Of these, 98 probes (representing 85 genes) were at least 10-fold (up or down) differentially expressed ($P_{adj} < 0.01$) between the two cell types. Selected genes playing a role in MDSC differentiation are shown in Fig. 3. We found that SK-MEL-5-educated M-MDSCs showed significant upregulation of *CSF2* (*GM-CSF*) and *CSF1* (*M-CSF*) compared with monocytes across all 4 donors tested (Fig. 3A–C). These results are in line with previous findings that the expansion of immature myeloid cells is mediated largely by CSF2, CSF1, and other growth factors produced by tumor cells and tumor stroma (17). In addition, SK-MEL-5-educated M-MDSCs expressed the *FLT1* receptor (*VEGFR1*), previously identified to enable VEGF to function as a chemoattractant for MDSCs (Fig. 3A and D; ref. 39). Consistent with previous findings, we identified *MMP9*, a matrix-degrading enzyme highly expressed in SK-MEL-5-educated M-MDSCs compared with monocytes, that promotes

angiogenesis and metastasis (Fig. 3A and E; ref. 40). In addition, we found that SK-MEL-5-educated M-MDSCs have increased levels of *IL6* and indole amine 2,3 dioxygenase (*IDO1*), which have been reported to induce the immunosuppressive effects of MDSCs (Fig. 3A, F, and G; ref. 41). The expression of *STAT1* mRNA was also upregulated in SK-MEL-5-educated M-MDSCs compared with monocytes. Several studies have linked the activation of *STAT1* with suppressive phenotype of MDSCs (Fig. 3A and H; ref. 42). Accumulation of M-MDSC has been reported to be dependent on *STAT1*, as reduced MDSC levels were observed in tumor-bearing mice deficient in *STAT1* (43). We found that SK-MEL-5-educated M-MDSCs exhibited significantly higher expression of *CD274* (*PDL1*) and *PDCD1LG2* (*PDL2*) compared with monocytes (Fig. 3A, I and J). A 2016 study reported that *PDL1*⁺ M-MDSCs accumulate in human cancers, including colorectal cancer, and might inhibit activation and function of tumor-infiltrating CTLs in the TME because of higher expression of *PDL1* (44). We found that *ILT3* (*LILRB4*), *CXCL10*, *CCL2* (*MCP1*), and *CCL22* (*MDC*) expression was significantly elevated in SK-MEL-5-educated M-MDSCs compared with monocytes (Fig. 3A and K; Supplementary Fig. S7A–S7C). *IL10* levels were upregulated (~two-fold) in SK-MEL-5-educated M-MDSCs in 2 of 4 donors (data not shown), and costimulatory molecule *CD86* and *STAT6* levels were downregulated in M-MDSCs compared with monocytes (Fig. 3A; Supplementary Fig. S7D and S7E). *CD163* has been reported to be a marker associated with human M2 macrophages (45). Our results show that compared with monocytes, SK-MEL-5-educated M-MDSCs had higher expression of *CD163* (Fig. 3A; Supplementary Fig. S7F).

ILT3 antagonism alters maturation and activation of M-MDSC

Recently, much effort has been made to understand how MDSCs exert immunosuppressive effects, including the concept that *ILT3* expression can serve to keep myeloid cells in an immature and suppressive state (32). To investigate this in our model, we assessed the binding of anti-*ILT3* antibody c52B8 to *ILT3* expressed on the cell surface by flow cytometry in human CD14⁺ cells from whole blood, frozen PBMCs, and SK-MEL-5-educated M-MDSCs. An IgG4 chimeric variant of clone 52B8 binds with high affinity to M-MDSCs (range EC₅₀ 55–60 ng/mL), similar to its binding of human peripheral blood CD14⁺ monocytes (EC₅₀ 13–41 ng/mL; Table 1).

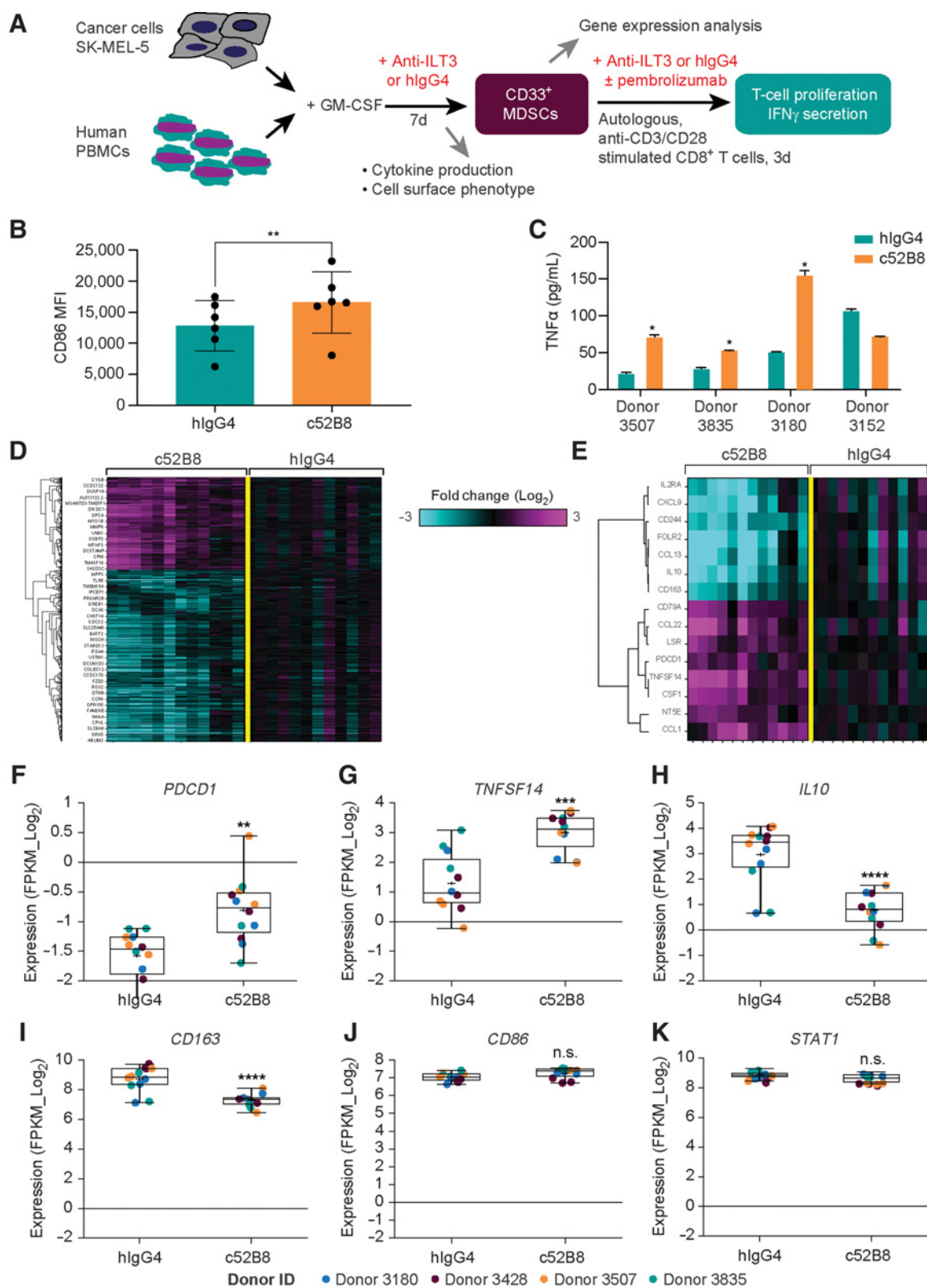
We next explored whether this antibody could impact M-MDSC maturation during differentiation (Fig. 4A). The cells were differentiated in the presence of isotype control hIgG4 or anti-*ILT3* antibody c52B8. We found that M-MDSCs differentiated in the presence of anti-*ILT3* have modest and consistent increases in the activation marker *CD86* as observed by increased staining compared with cells treated with isotype control hIgG4 (Fig. 4B). We then examined proinflammatory cytokine secretion in conditioned media from M-MDSC cocultures. In comparison with the control antibody, anti-*ILT3* increased TNF α levels in conditioned media from M-MDSC cocultures in 3 of 4 PBMC donors (Fig. 4C). We found that anti-*ILT3* could

Table 1. Binding of anti-*ILT3* to human primary cells and *in vitro* differentiated SK-MEL-5-educated human M-MDSCs.

Test Article (Lot no.)	Samples tested	Donor ID	EC ₅₀ (ng/mL)
c52B8 (42APB)	Fresh CD14 ⁺ monocytes from whole blood	Human donor #851	41
	CD14 ⁺ monocytes from frozen PBMC	Human donor #3608	13
	Monocyte-derived suppressor cells	Human donor #3507	55
		Human donor #3180	60

Abbreviation: EC₅₀, half-maximal effective concentration(s).

Downloaded from http://aacrjournals.org/mcr/article-pdf/19/4/702/3101820/702.pdf by guest on 10 February 2024



modulate the phenotype of these suppressive myeloid cells to promote a mature and activated phenotype, determined by CD86 activation and increased levels of secreted TNF α .

Furthermore, we examined the transcriptional changes in immunosuppressive SK-MEL-5-educated M-MDSCs treated with anti-ILT3 antibody c52B8 or isotype control hIgG4 antibody to identify differentially expressed genes (DEG) using RNA-seq analysis. Comparison of anti-ILT3-treated vs. hIgG4-treated SK-MEL-5-educated M-MDSCs identified 623 DEGs (219 upregulated and 404 downregulated) when combining all 4 donors [at least ± 1.5 -fold change with P_{adj} (FDR) < 0.01 , and removing low expressed genes, see Methods; Fig. 4D and E; Supplementary Table S3]. To determine potential biological process related to immunosuppressive phenotype of SK-MEL-5-educated M-MDSCs, we performed gene ontology (GO) enrichment pathway analysis on 623 genes. We found immune response GO terms were enriched in this signature (Supplementary Table S4). Anti-ILT3 increased *PDCD1* (*PD1*) and *TNFSF14* expression in SK-MEL-5-educated M-MDSCs compared with isotype control (Fig. 4F and G). The expression of suppressive molecules, such as *IL10* and *CD163*, were diminished in SK-MEL-5-educated M-MDSCs in response to anti-ILT3 compared with isotype control (Fig. 4H and I).

Several mechanisms by which IL10 inhibits T-cell-mediated anti-tumor immune responses in the TME has been proposed, including suppression of IFN γ -dependent activation of APCs with decreased expression of MHC II and CD86 and inhibition of CD28 costimulatory pathway (46, 47).

We observed an upregulation of the costimulatory molecule CD86 levels in M-MDSCs treated with anti-ILT3 when compared with isotype control, but it was not significant (Fig. 4J). Similarly, we observed a trend toward downregulation of *STAT1* expression following treatment with anti-ILT3 in SK-MEL-5-educated M-MDSCs (Fig. 4K).

ILT3 antagonism reverses M-MDSC-induced suppression of effector T cells

Previous studies have shown that MDSCs can inhibit effector T-cell responses, using a variety of mechanisms, including IL10 secretion, PDL1/L2 expression, and cytokine-dependent Treg conversion (48). Because ILT3 is expressed on these cells, we hypothesized that ILT3⁺ MDSCs may cause suppression of T-cell activation and proliferation. To test the effect of MDSCs matured in the presence of anti-ILT3 on T-cell responses, we performed MDSC/T-cell suppression assays. We cultured human PBMCs with SK-MEL-5 tumor cells and GM-CSF for 7 days. SK-MEL-5-educated CD33⁺ cells were collected by positive antibody-based magnetic bead selection and then cocultured with purified autologous CD8⁺ T cells at a ratio of 2:1, 4:1, and 8:1 (T cell: MDSC) for 3 days in the presence of a polyclonal stimulus. Similar concentration of anti-ILT3 antibody c52B8 or isotype control antibody

was added in both the coculture and T-cell suppression steps. The suppressive effect of anti-ILT3 matured MDSCs on T cells was evaluated by IFN γ levels in the supernatants secreted by T cells. The MDSCs generated in the presence of anti-ILT3 showed modest but consistent effect in reversal of T-cell suppression measured by increase in IFN γ secretion, indicating that anti-ILT3 reduced the suppressive capacity of M-MDSCs as compared with isotype control treatment. Overall, the effects were most noticeable at 4 T cell:1 MDSC ratio in three-quarters of PBMC donors (Fig. 5A–D). We showed that ILT3 antagonism induced the phenotype of more mature myeloid cells that enhanced effector T-cell response.

Next, we examined whether anti-ILT3 has an effect during acquisition of MDSCs or during T-cell suppression or both. To address these questions, antibody was added to the cocultures of SK-MEL-5 and PBMCs at different stages of experimentation: (i) during differentiation, but not during T-cell suppression, (ii) during T-cell suppression but not during MDSC differentiation, and (iii) during both steps (MDSC differentiation and T-cell suppression).

We found that the addition of anti-ILT3 antibody c52B8 to the coculture of PBMCs and SK-MEL-5 cells during the differentiation step resulted in only a modest but consistent decrease in the suppressive capacity of CD33⁺ cells purified from those cocultures. Addition of anti-ILT3 during only the T-cell suppression step was not efficacious, and addition of anti-ILT3 during both the differentiation and T-cell suppression steps showed similar effect as observed with the addition of antibody during only the differentiation step (Table 2).

Addition of antibody during only the differentiation step caused 22% T-cell suppression at 4 T cell:1 MDSC ratio compared with 43% T-cell suppression when antibody was added during only the T-cell suppression stage. Also, addition of anti-ILT3 during both the differentiation and T-cell suppression steps caused 17% T-cell suppression compared with 55% with hIgG4 isotype control (Table 2). We, therefore, concluded that anti-ILT3 impaired the acquisition of the suppressive phenotype of SK-MEL-5-educated M-MDSCs.

Anti-ILT3 combines with pembrolizumab to enhance effector T-cell function

We observed that PD1 and PDL1 protein expression is upregulated on the surface of human CD8⁺T cells stimulated with anti-CD3/CD28 antibody-coupled beads, suggesting potential for a combination with pembrolizumab (Fig. 6A and B). We also noted that PD1 mRNA expression is upregulated in SK-MEL-5-educated M-MDSCs following treatment with anti-ILT3 antibody (Fig. 4F). These findings were similar to those in a recent study by Strauss and colleagues (49). They showed that even with conserved PD1 expression in T cells, myeloid cell-specific PD1 knockout resulted in an increase of T effector memory cells with enhanced functionality and mediated antitumor protection (49). The combination effect of anti-ILT3 antibody with pembrolizumab on function of M-MDSCs was assessed in MDSC and

Figure 4.

ILT3 antagonism promotes maturation and activation of SK-MEL-5-educated M-MDSCs. **A**, Method for evaluating effect of anti-ILT3 antibody on the acquisition of functional phenotypes in monocytic MDSCs. **B**, Analysis of activation marker CD86 on M-MDSCs analyzed by flow cytometry MFI (mean fluorescence intensity), following treatment with hIgG4 or anti-ILT3 c52B8 ($n = 6$ PBMC donors), and P value was calculated using paired t test (**, $P < 0.005$). **C**, Representative histogram showing secreted TNF α levels in PBMC/SK-MEL-5 cocultures following treatment with hIgG4 (green bar) or anti-ILT3 c52B8 (yellow bar). The results are expressed as average \pm SD from two technical replicates ($n = 4$ PBMC donors), and P value was calculated using paired t test (*, $P < 0.05$). **D** and **E**, ILT3 blockade alters the M-MDSC transcriptome. Shown in the heatmap in **D** are the 623 genes significantly regulated by anti-ILT3 c52B8 treatment compared with isotype control hIgG4 treatment in M-MDSCs (1.5 \times and FDR < 0.05 , GrpMaxNormCount > 50). The color gradient represents the log₂ fold change of each individual sample (each column) treated with anti-ILT3 c52B8 compared with the corresponding pooled control samples treated with isotype control hIgG4 as baseline ($\pm \log_2(3)$ fold). A subset of genes are highlighted in the heatmap in **E**. **F–K**, Gene expression levels (FPKM, log₂) of *PDCD1* (*PD1*), *TNFSF14*, *IL10*, *CD163*, *CD86*, and *STAT1* in M-MDSCs in the presence of hIgG4 or anti-ILT3 c52B8 ($n = 4$ PBMC donors). Adjusted P value was calculated using R package DESeq2 (v1.22.2). **, $P < 0.005$; ***, $P < 0.0005$; ****, $P < 0.0001$; n.s., not statistically significant.

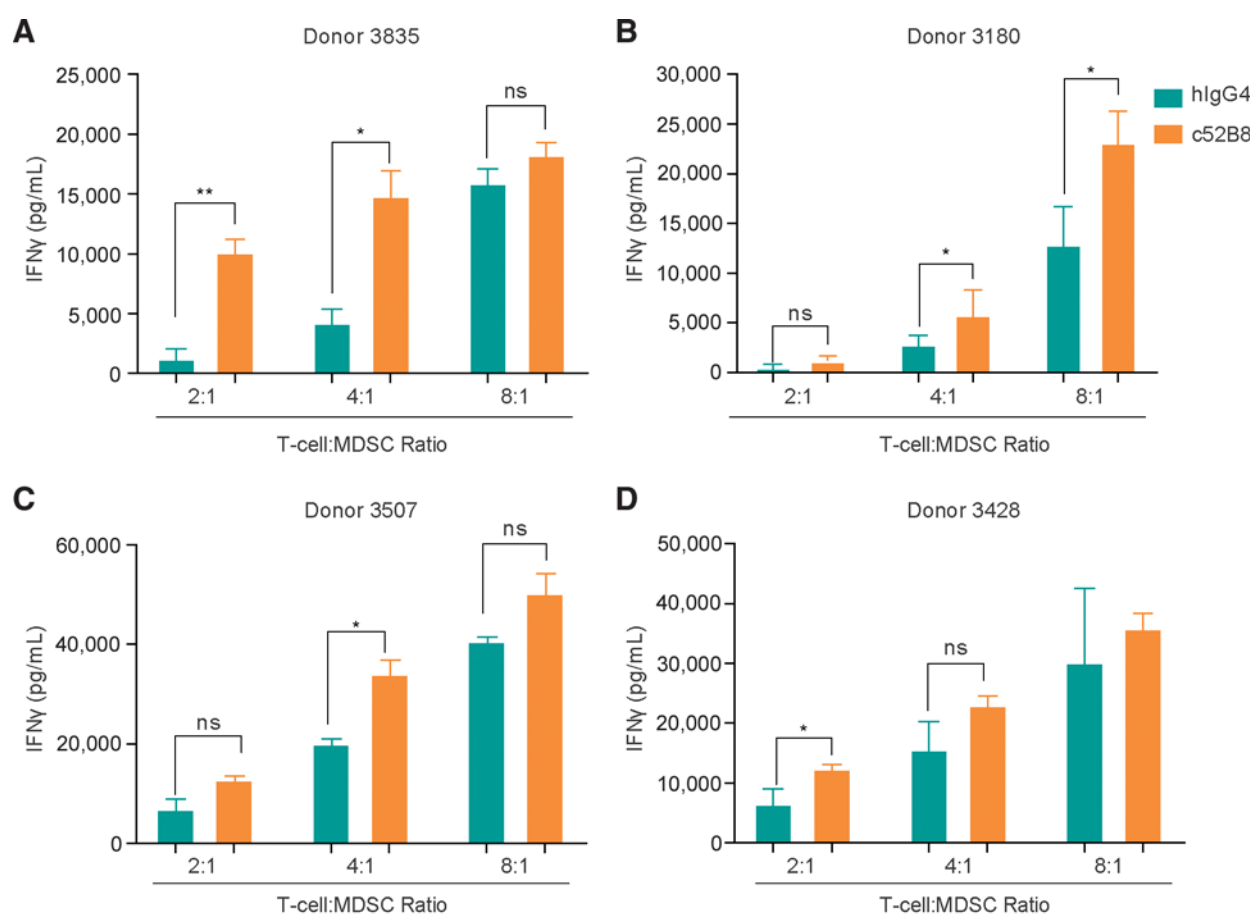


Figure 5.

SK-MEL-5-educated M-MDSCs differentiated in the presence of anti-ILT3 antibody c52B8 are less suppressive compared with isotype control hlgG4 antibody-treated cells. **A–D**, Representative histogram showing secreted IFN γ levels in anti-CD3/CD28 stimulated M-MDSC/T-cell cocultures following treatment with isotype control hlgG4 (light green bar) or anti-ILT3 (orange bar). The data shown are average and SD of $n = 3$ technical replicates at the level of the T-cell assay step ($n = 4$ PBMC donors), and paired t test was used to calculate P value (*, $P < 0.05$; **, $P < 0.005$; n.s., not statistically significant).

T-cell cocultures. We cultured autologous CD8⁺ T cells isolated from healthy human PBMCs with SK-MEL-5-educated CD33⁺ MDSCs at the ratio of 8:1. The cocultures were treated with isotype control antibody hlgG4, pembrolizumab only, or anti-ILT3 antibody h52B8 (humanized IgG4 variant) only, or the combination of anti-ILT3 and pembrolizumab. Analyses of supernatants from cocultures showed that treatment with anti-ILT3 plus pembrolizumab caused a significant increase in IFN γ levels compared with cultures treated with either anti-ILT3 or pembrolizumab only. We concluded that anti-ILT3 synergized with pembrolizumab to enhance effector T-cell secretion of IFN γ (Fig. 6C).

Discussion

In recent years, MDSCs have gained importance with respect to influencing the outcome of checkpoint inhibition therapy because they have been reported to suppress T-cell responses in patients with cancer (6, 50). The mechanisms of their accumulation and ability to suppress immune cell function, however, are poorly understood. Human MDSCs comprise a diverse group of suppressive cells that have been difficult to characterize owing to their plastic nature.

In this study, we demonstrate that highly immunosuppressive human M-MDSCs can be generated *in vitro* by coculturing healthy

Table 2. Effect of anti-ILT3 on the acquisition of SK-MEL-5-educated human M-MDSCs.

(4:1) T cell: MDSC ratio		During differentiation (7d)	During T-cell assay (3d)	% Suppression ^a
Anti-ILT3 7d +	IgG4 3d	Anti-ILT3	IgG4	22 ± 2.05
IgG4 7d +	Anti-ILT3 3d	IgG4	Anti-ILT3	43 ± 10.69
Anti-ILT3 10d		Anti-ILT3	Anti-ILT3	17 ± 3.46
IgG4 10d		IgG4	IgG4	55 ± 1.69

^aThe data shown are average, and SD of $n = 3$ technical replicates at the level of the T-cell assay step. ($n = 2$ PBMC donors).

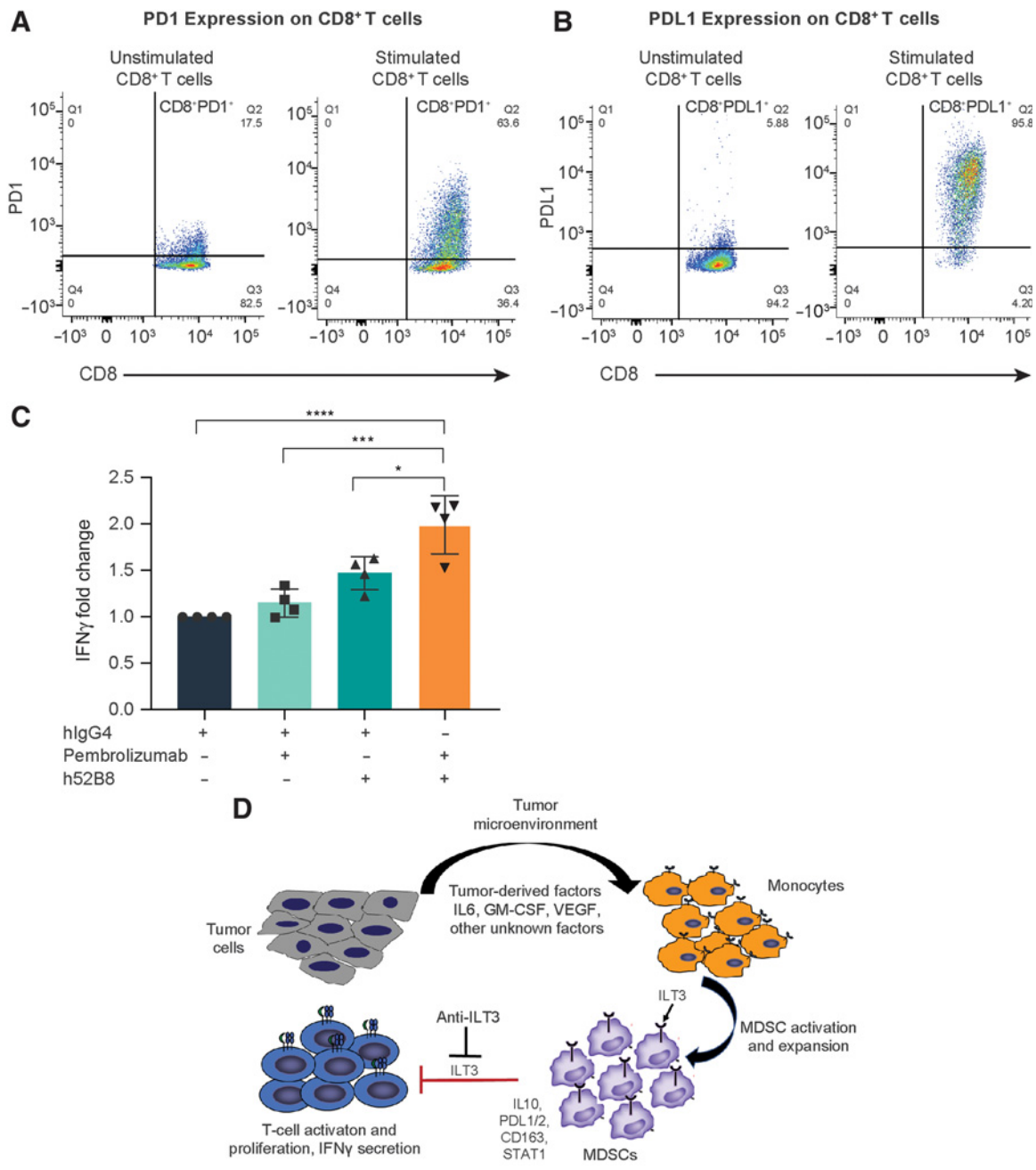


Figure 6.

Anti-ILT3 combines with pembrolizumab in reversing M-MDSC-induced T-cell suppression. **A**, Analysis of PD1 expression on CD8⁺T cells analyzed by flow cytometry MFI (mean fluorescence intensity), following stimulation with anti-CD3/CD28 beads. **B**, Analysis of PD-L1 expression on CD8⁺T cells analyzed by flow cytometry (MFI) following stimulation with anti-CD3/CD28 beads. **C**, Representative histogram showing secreted IFN γ levels in anti-CD3/CD28 stimulated M-MDSC/T-cell cocultures following treatment with hlgG4 (gray bar) or pembrolizumab (light green bar) or anti-ILT3 antibody h52B8 (dark green bar), or combination of anti-ILT3 h52B8 and pembrolizumab (orange bar). Data are representative of 4 PBMC donors. The results are expressed as average \pm SD from four technical replicates in each experiment, and one-way ANOVA followed by Tukey multiple-comparisons test was used to calculate *P* value (*, *P* < 0.05; ***, *P* < 0.0005; ****, *P* < 0.0001). **D**, Proposed potential mechanism of MDSC-mediated T-cell suppression through ILT3 (LILRB4). Tumor-derived factors induce differentiation of monocytes to immunosuppressive MDSCs. Tumor-educated MDSCs express inhibitory receptor ILT3-promoting myeloid cell tolerance and immunosuppression. Targeting ILT3 can reprogram inhibitory tumor-associated suppressive myeloid cells into anticancer immune response stimulators.

human PBMCs with a tumor cell line SK-MEL-5. The SK-MEL-5-educated M-MDSCs exhibited decreased cell surface expression of HLA-DR and the ability to functionally inhibit CD8⁺T-cell activation and proliferation.

Moreover, in our study, SK-MEL-5-educated M-MDSCs expressed *VEGFR1* and *MMP9*, essential mediators of neoangiogenesis and tissue invasion at the tumor site. This supports findings from previous studies stating that MDSCs are capable of supporting tumor growth

through remodeling of the TME (5, 16, 17). Emerging data indicates that MDSCs can confer resistance to antiangiogenic therapies (51). Recent studies have shown a decrease in the number of circulating MDSCs that were found in patients with cancer, when treated with sunitinib, a multikinase inhibitor with antiangiogenic activity (52). It has been demonstrated in preclinical studies that sunitinib can deplete MDSCs both in circulation and in tumors (53).

Activation of immune cells involves a cascade of signaling events downstream of receptor engagement with the appropriate ligand(s). Receptor activity is often controlled by the presence of cytoplasmic immunoreceptor tyrosine-based activation or inhibitory motifs (ITAMs or ITIMs). A class of surface receptors belonging to the immunoglobulin superfamily called the ILTs or LILRs have been reported to be regulated in a similar way. One such family member, ILT3, is expressed on myeloid APCs and has been shown to function as an inhibitory receptor owing to the putative ITIMs on its cytoplasmic tail. Particularly in the context of cancer, ILT3 has been reported to be expressed by tolerogenic dendritic cells (DC) and MDSCs and negatively correlates with patient survival (29). The main mechanisms reported to date are T-cell suppression and induction of regulatory T cells (54–57). In line with these findings, we show for the first time that SK-MEL-5-educated M-MDSCs express high levels of the immunoinhibitory receptor ILT3.

Our data show that ILT3 antagonism by a specific mAb promotes inflammatory responses and mature phenotypes in SK-MEL-5-educated M-MDSCs. We found that TNF α levels in PBMC and SK-MEL-5 coculture supernatant were higher after treatment with anti-ILT3 compared with isotype control antibody (Fig. 4C). This observation was consistent with a more activated, less suppressive phenotype of the anti-ILT3-treated M-MDSCs. ILT3 blockade decreased the expression of suppressive molecules *CD163* and *IL10* while promoting activation marker *CD86* in SK-MEL-5-educated M-MDSCs during differentiation, suggesting that ILT3 antagonism drives MDSCs toward a mature activated phenotype. It appears that *STAT1* levels are downregulated following treatment with anti-ILT3 in SK-MEL-5-educated M-MDSCs (Fig. 4K), and this trend has been proposed to have a role in MDSC accumulation in tumors. Hix and colleagues reported that ectopic overexpression of constitutively active *STAT1* in breast cancer cells promoted infiltration of MDSCs and inhibition of tumor-specific T cells, resulting in aggressive tumor growth in tumor-transplanted, immune-competent mice (43). In addition, ILT3 antagonism partially reversed the immunosuppressive functions of SK-MEL-5-educated M-MDSCs across donors. Two recent studies have shown similar findings in AML, in which ILT3-mediated T-cell suppression was reversed by anti-ILT3 blocking antibodies (58, 59). Most importantly, we showed that ILT3 antagonism in combination with anti-PD1 enhanced T-cell activation as assessed by IFN γ secretion *in vitro*. It would be interesting to further explore anti-ILT3 in combination with chemotherapies, T-cell and myeloid checkpoint blockers, and other immune therapies. In addition, we found that *CCL22* expression was elevated in SK-MEL-5-educated M-MDSCs compared with monocytes. Recent studies have shown that regulatory T cells are recruited through *CCL22/CCR4* in tumors resulting in the prevention of effector T-cell activation,

immune escape, and tumor progression (60). Because the expression of *CCL22* is further increased in SK-MEL-5-educated M-MDSCs following treatment with anti-ILT3, maybe blockade of *CCL22* in combination with anti-ILT3 and anti-PD1 would increase the number of tumor infiltrating activated CD8⁺T cells and improved antitumor immune responses. This combination will be tested in the future.

From this study, we are able to propose a model for the induction and function of monocytic MDSCs generated in tumors (Fig. 6D). This model embodies a role for tumor-derived cytokines, the inhibitory receptor ILT3, and signaling of the suppressive molecules IL10, *CD163*, and *STAT1* in myeloid cells. We further show that ILT3 blockade inhibits the acquisition of the suppressive phenotype of tumor-educated M-MDSCs. Blockade of ILT3 can reprogram immunosuppressive tumor-associated M-MDSCs to an immunostimulatory phenotype and can be used in combination with checkpoint blockade to improve the therapeutic outcome through modulation of the TME. Finally, we suggest that the model of primary human M-MDSCs described in this study is a useful platform for studying novel therapeutic strategies focusing on M-MDSC-related effects in cancer.

Authors' Disclosures

L. Singh reports a patent for "Antibodies Specific For Immunoglobulin-Like Transcript 3 (ILT3) and uses thereof pending"; in addition, L. Singh is an employee of Merck & Co. Inc. E.S. Muise is an employee of Merck & Co. Inc. A. Bhattacharya reports other from Merck & Co during the conduct of the study; other from Merck & Co outside the submitted work. C. Zhang reports other from Merck outside the submitted work. D.Y. Chiang reports personal fees from Merck outside the submitted work. S.H. Ranganath is an employee of Merck and Co. No disclosures were reported by the other authors.

Authors' Contributions

L. Singh: Conceptualization, formal analysis, investigation, methodology, writing—original draft, writing—review and editing. **E.S. Muise:** Data curation, formal analysis, investigation, visualization, writing—review and editing. **A. Bhattacharya:** Formal analysis, writing—review and editing. **J. Grein:** Formal analysis, investigation, methodology. **S. Javai:** Data curation, formal analysis, investigation, visualization. **P. Stivers:** Formal analysis, validation, investigation. **J. Zhang:** Formal analysis, validation, investigation. **Y. Qu:** Investigation, methodology. **B. Joyce-Shaikh:** Investigation, methodology. **A. Loboda:** Data curation, formal analysis, writing—review and editing. **C. Zhang:** Data curation, formal analysis, investigation, visualization. **M. Meehl:** Conceptualization, methodology, generation of anti-ILT3 antibody. **D.Y. Chiang:** Data curation, formal analysis. **S.H. Ranganath:** Writing—review and editing. **M. Rosenzweig:** Writing—review and editing. **P.E. Brandish:** Conceptualization, supervision, writing—review and editing.

Acknowledgments

We would like to thank Drs. W. Nicholas Haining and Jie Zhang-Hoover for their review of the manuscript and valuable input. We acknowledge Marc Alexander Sze for input on scRNAseq data interpretation in NSCLC public datasets and Anthony Palmieri for suggestions on data analysis.

The costs of publication of this article were defrayed in part by the payment of page charges. This article must therefore be hereby marked *advertisement* in accordance with 18 U.S.C. Section 1734 solely to indicate this fact.

Received July 15, 2020; revised October 28, 2020; accepted December 17, 2020; published first December 28, 2020.

References

- Sharma P, Allison JP. The future of immune checkpoint therapy. *Science* 2015; 348:56–61.
- Topalian SL, Drake CG, Pardoll DM. Immune checkpoint blockade: a common denominator approach to cancer therapy. *Cancer Cell* 2015;27:450–61.
- Cassetta L, Pollard JW. Targeting macrophages: therapeutic approaches in cancer. *Nat Rev Drug Discov* 2018;17:887–904.
- DeNardo DG, Ruffell B. Macrophages as regulators of tumour immunity and immunotherapy. *Nat Rev Immunol* 2019;19:369–82.

5. Groth C, Hu X, Weber R, Fleming V, Altevogt P, Utikal J, et al. Immunosuppression mediated by myeloid-derived suppressor cells (MDSCs) during tumour progression. *Br J Cancer* 2019;120:16–25.
6. Meyer C, Cagnon L, Costa-Nunes CM, Baumgaertner P, Montandon N, Leyvraz L, et al. Frequencies of circulating MDSC correlate with clinical outcome of melanoma patients treated with ipilimumab. *Cancer Immunol Immunother* 2014;63:247–57.
7. Zilionis R, Engblom C, Pfirschke C, Savova V, Zemmour D, Saatcioglu HD, et al. Single-cell transcriptomics of human and mouse lung cancers reveals conserved myeloid populations across individuals and species. *Immunity* 2019;50:1317–34.
8. Chevrier S, Levine JH, Zanotelli VRT, Silina K, Schulz D, Bacac M, et al. An immune atlas of clear cell renal cell carcinoma. *Cell* 2017;169:736–49.
9. Consonni FM, Porta C, Marino A, Pandolfo C, Mola S, Bleve A, et al. Myeloid-derived suppressor cells: ductile targets in disease. *Front Immunol* 2019;10:949.
10. Condamine T, Mastio J, Gabrilovich DI. Transcriptional regulation of myeloid-derived suppressor cells. *J Leukoc Biol* 2015;98:913–22.
11. Ostrand-Rosenberg S, Sinha P. Myeloid-derived suppressor cells: linking inflammation and cancer. *J Immunol* 2009;182:4499–506.
12. Okada SL, Simmons RM, Franke-Welch S, Nguyen TH, Korman AJ, Dillon SR, et al. Conditioned media from the renal cell carcinoma cell line 786.O drives human blood monocytes to a monocytic myeloid-derived suppressor cell phenotype. *Cell Immunol* 2018;323:49–58.
13. Zhang B, Wang Z, Wu L, Zhang M, Li W, Ding J, et al. Circulating and tumor-infiltrating myeloid-derived suppressor cells in patients with colorectal carcinoma. *PLoS One* 2013;8:e57114.
14. Vasquez-Dunddel D, Pan F, Zeng Q, Gorbounov M, Albesiano E, Fu J, et al. STAT3 regulates arginase-I in myeloid-derived suppressor cells from cancer patients. *J Clin Invest* 2013;123:1580–9.
15. Sharma P BA, Necchi A, Plimack ER, Pal SK, Bedke J, et al., editors. Abstract CT178: Nivolumab monotherapy in patients with advanced platinum-resistant urothelial carcinoma: Efficacy and safety update and association between biomarkers and overall survival in CheckMate 275 [abstract]. In: Proceedings of the American Association for Cancer Research Annual Meeting 2018; Apr 14–18; Chicago, IL. Philadelphia (PA): AACR; 2018. Abstract nr CT178.
16. Kumar V, Patel S, Tcyganov E, Gabrilovich DI. The nature of myeloid-derived suppressor cells in the tumor microenvironment. *Trends Immunol* 2016;37:208–20.
17. Marvel D, Gabrilovich DI. Myeloid-derived suppressor cells in the tumor microenvironment: expect the unexpected. *J Clin Invest* 2015;125:3356–64.
18. Bronte V, Brandau S, Chen SH, Colombo MP, Frey AB, Greten TF, et al. Recommendations for myeloid-derived suppressor cell nomenclature and characterization standards. *Nat Commun* 2016;7:12150.
19. Gabrilovich DI, Ostrand-Rosenberg S, Bronte V. Coordinated regulation of myeloid cells by tumours. *Nat Rev Immunol* 2012;12:253–68.
20. Gabrilovich DI, Nagaraj S. Myeloid-derived suppressor cells as regulators of the immune system. *Nat Rev Immunol* 2009;9:162–74.
21. Lechner MG, Liebertz DJ, Epstein AL. Characterization of cytokine-induced myeloid-derived suppressor cells from normal human peripheral blood mononuclear cells. *J Immunol* 2010;185:2273–84.
22. Lechner MG, Megiel C, Russell SM, Bingham B, Arger N, Woo T, et al. Functional characterization of human Cd33+ and Cd11b+ myeloid-derived suppressor cell subsets induced from peripheral blood mononuclear cells cocultured with a diverse set of human tumor cell lines. *J Transl Med* 2011;9:90.
23. Mao Y, Poschke I, Wennerberg E, Pico de Coana Y, Egyhazi Brage S, Schultz I, et al. Melanoma-educated CD14+ cells acquire a myeloid-derived suppressor cell phenotype through COX-2-dependent mechanisms. *Cancer Res* 2013;73:3877–87.
24. Mahne AE, Mauze S, Joyce-Shaikh B, Xia J, Bowman EP, Beebe AM, et al. Dual roles for regulatory T-cell depletion and costimulatory signaling in agonistic GITR targeting for tumor immunotherapy. *Cancer Res* 2017;77:1108–18.
25. Zhang J, Mai S, Chen HM, Kang K, Li XC, Chen SH, et al. Leukocyte immunoglobulin-like receptors in human diseases: an overview of their distribution, function, and potential application for immunotherapies. *J Leukoc Biol* 2017;102:351–60.
26. Ma G, Pan PY, Eisenstein S, Divino CM, Lowell CA, Takai T, et al. Paired immunoglobulin-like receptor-B regulates the suppressive function and fate of myeloid-derived suppressor cells. *Immunity* 2011;34:385–95.
27. Kostlin N, Ostermeir AL, Spring B, Schwarz J, Marme A, Walter CB, et al. HLA-G promotes myeloid-derived suppressor cell accumulation and suppressive activity during human pregnancy through engagement of the receptor ILT4. *Eur J Immunol* 2017;47:374–84.
28. Kang X, Kim J, Deng M, John S, Chen H, Wu G, et al. Inhibitory leukocyte immunoglobulin-like receptors: immune checkpoint proteins and tumor sustaining factors. *Cell Cycle* 2016;15:25–40.
29. de Goeje PL, Bezemer K, Heuvers ME, Dingemans AC, Groen HJ, Smit EF, et al. Immunoglobulin-like transcript 3 is expressed by myeloid-derived suppressor cells and correlates with survival in patients with non-small cell lung cancer. *Oncoimmunology* 2015;4:e1014242.
30. Cella M, Dohring C, Samaridis J, Dessing M, Brockhaus M, Lanzavecchia A, et al. A novel inhibitory receptor (ILT3) expressed on monocytes, macrophages, and dendritic cells involved in antigen processing. *J Exp Med* 1997;185:1743–51.
31. Lu HK, Rentero C, Raftery MJ, Borges L, Bryant K, Tedla N. Leukocyte Ig-like receptor B4 (LILRB4) is a potent inhibitor of FcγRI-mediated monocyte activation via dephosphorylation of multiple kinases. *J Biol Chem* 2009;284:34839–48.
32. Xu Z, Ho S, Chang CC, Zhang QY, Vasilescu ER, Vlad G, et al. Molecular and cellular characterization of human CD8 T suppressor cells. *Front Immunol* 2016;7:549.
33. Meehl MA, Brandish PE, Fayadat-Dilman L, Juan V, Mieczkowski C, Singh L, inventors; Merck, Sharpe & Dohme, assignee. Antibodies specific for immunoglobulin-like transcript 3 (ILT3) and uses thereof. US Patent Application No US 2019/0153093 A1. 2019 May 23.
34. de Fries R, Mitsuhashi M. Quantification of mitogen induced human lymphocyte proliferation: comparison of alamarBlue assay to 3H-thymidine incorporation assay. *J Clin Lab Anal* 1995;9:89–95.
35. Zhou X, Muise ES, Haimbach R, Sebhat IK, Zhu Y, Liu F, et al. PAN-AMPK activation improves renal function in a rat model of progressive diabetic nephropathy. *J Pharmacol Exp Ther* 2019;371:45–55.
36. Tomic S, Joksimovic B, Bekic M, Vasiljevic M, Milanovic M, Colic M, et al. Prostaglandin-E2 potentiates the suppressive functions of human mononuclear myeloid-derived suppressor cells and increases their capacity to expand IL-10-producing regulatory T cell subsets. *Front Immunol* 2019;10:475.
37. Newman AM, Liu CL, Green MR, Gentles AJ, Feng W, Xu Y, et al. Robust enumeration of cell subsets from tissue expression profiles. *Nat Methods* 2015;12:453–7.
38. Nagaraj S, Youn JI, Gabrilovich DI. Reciprocal relationship between myeloid-derived suppressor cells and T cells. *J Immunol* 2013;191:17–23.
39. Parker KH, Beury DW, Ostrand-Rosenberg S. Myeloid-derived suppressor cells: critical cells driving immune suppression in the tumor microenvironment. *Adv Cancer Res* 2015;128:95–139.
40. Tartour E, Pere H, Maillere B, Terme M, Merillon N, Taieb J, et al. Angiogenesis and immunity: a bidirectional link potentially relevant for the monitoring of antiangiogenic therapy and the development of novel therapeutic combination with immunotherapy. *Cancer Metastasis Rev* 2011;30:83–95.
41. Smith C, Chang MY, Parker KH, Beury DW, DuHadaway JB, Flick HE, et al. IDO is a nodal pathogenic driver of lung cancer and metastasis development. *Cancer Discov* 2012;2:722–35.
42. Movahedi K, Guillemins M, Van den Bossche J, Van den Bergh R, Gysemans C, Beschin A, et al. Identification of discrete tumor-induced myeloid-derived suppressor cell subpopulations with distinct T cell-suppressive activity. *Blood* 2008;111:4233–44.
43. Hix LM, Karavitis J, Khan MW, Shi YH, Khazaie K, Zhang M. Tumor STAT1 transcription factor activity enhances breast tumor growth and immune suppression mediated by myeloid-derived suppressor cells. *J Biol Chem* 2013;288:11676–88.
44. Lu C, Redd PS, Lee JR, Savage N, Liu K. The expression profiles and regulation of PD-L1 in tumor-induced myeloid-derived suppressor cells. *Oncoimmunology* 2016;5:e1247135.
45. Biswas SK, Mantovani A. Macrophage plasticity and interaction with lymphocyte subsets: cancer as a paradigm. *Nat Immunol* 2010;11:889–96.
46. Mittal SK, Cho KJ, Ishido S, Roche PA. Interleukin 10 (IL-10)-mediated immunosuppression: MARCH-I induction regulates antigen presentation by macrophages but not dendritic cells. *J Biol Chem* 2015;290:27158–67.
47. Taylor A, Verhagen J, Blaser K, Akdis M, Akdis CA. Mechanisms of immune suppression by interleukin-10 and transforming growth factor-beta: the role of T regulatory cells. *Immunology* 2006;117:433–42.
48. Han S, Yang Y. Phenotypic and functional dissection of myeloid-derived suppressor cells. *Appl Biol Chem* 2016;59:367–71.

49. Strauss L, Mahmoud MAA, Weaver JD, Tijaro-Ovalle NM, Christofides A, Wang Q, et al. Targeted deletion of PD-1 in myeloid cells induces antitumor immunity. *Sci Immunol* 2020;5:eaay1863.
50. Messmer MN, Netherby CS, Banik D, Abrams SI. Tumor-induced myeloid dysfunction and its implications for cancer immunotherapy. *Cancer Immunol Immunother* 2015;64:1–13.
51. Horikawa N, Abiko K, Matsumura N, Baba T, Hamanishi J, Yamaguchi K, et al. Anti-VEGF therapy resistance in ovarian cancer is caused by GM-CSF-induced myeloid-derived suppressor cell recruitment. *Br J Cancer* 2020;122:778–88.
52. Lu LC, Chang CJ, Hsu CH. Targeting myeloid-derived suppressor cells in the treatment of hepatocellular carcinoma: current state and future perspectives. *J Hepatocell Carcinoma* 2019;6:71–84.
53. Draghiciu O, Nijman HW, Hoogbeem BN, Meijerhof T, Daemen T. Sunitinib depletes myeloid-derived suppressor cells and synergizes with a cancer vaccine to enhance antigen-specific immune responses and tumor eradication. *Oncoimmunology* 2015;4:e989764.
54. Brenk M, Scheler M, Koch S, Neumann J, Takikawa O, Hacker G, et al. Tryptophan deprivation induces inhibitory receptors ILT3 and ILT4 on dendritic cells favoring the induction of human CD4+CD25+ Foxp3+ T regulatory cells. *J Immunol* 2009;183:145–54.
55. Chang CC, Ciubotariu R, Manavalan JS, Yuan J, Colovai AI, Piazza F, et al. Tolerization of dendritic cells by T(S) cells: the crucial role of inhibitory receptors ILT3 and ILT4. *Nat Immunol* 2002;3:237–43.
56. Steinbrink K, Graulich E, Kubsch S, Knop J, Enk AH. CD4(+) and CD8(+) anergic T cells induced by interleukin-10-treated human dendritic cells display antigen-specific suppressor activity. *Blood* 2002;99:2468–76.
57. Suci-Foca N, Feirt N, Zhang QY, Vlad G, Liu Z, Lin H, et al. Soluble Ig-like transcript 3 inhibits tumor allograft rejection in humanized SCID mice and T cell responses in cancer patients. *J Immunol* 2007;178:7432–41.
58. Deng M, Gui X, Kim J, Xie L, Chen W, Li Z, et al. LILRB4 signalling in leukaemia cells mediates T cell suppression and tumour infiltration. *Nature* 2018;562:605–9.
59. Gui X, Deng M, Song H, Chen Y, Xie J, Li Z, et al. Disrupting LILRB4/APOE interaction by an efficacious humanized antibody reverses T-cell suppression and blocks AML development. *Cancer Immunol Res* 2019;7:1244–57.
60. Wiedemann GM, Knott MM, Vetter VK, Rapp M, Haubner S, Fessler J, et al. Cancer cell-derived IL-1alpha induces CCL22 and the recruitment of regulatory T cells. *Oncoimmunology* 2016;5:e1175794.